Ann. For. Sci. 59 (2002) 767–776

DOI: 10.1051/forest:2002063

Original article

Predicting oak wood properties using X-ray inspection: representation, homogenisation and localisation. Part I: Digital X-ray imaging and representation by finite elements

Éric Badel* and Patrick Perré

Laboratoire d'Étude et de Recherche sur le Matériau Bois, UMR 1093 INRA/ENGREF/Université Henri Poincaré Nancy I, ENGREF, 14, rue Girardet, 54042 Nancy Cedex, France

(Received 8 January 2002; accepted 21 May 2002)

Abstract – This paper is the first part of a complete modelling where wood is a 2D composite material. It proposes a comprehensive approach to predict the elastic and shrinkage properties of oak wood in the transverse plane from the local properties of the anatomical tissues and the actual morphology of those tissues. Part I is devoted to the methodology of representation. According to oak anatomy, the representative elementary volume used in this work consists of one annual ring limited in the tangential direction by large zones of ray cells. A high-resolution digital X-ray imaging device was built to represent the spatial distribution of tissues directly from cross-sections of wood. A complete image processing, including image segmentation and partitioned boundaries of tissues (ray cells, big vessels, etc.), was developed; which makes it possible to build a finite element mesh from these images. Thanks to the control of mesh refinement, the number of triangular elements is minimized while a good description of the anatomical structure is obtained. Using these F.E. meshes, Part II will present the homogenization principle and a few examples of calculations of the properties. Macroscopic properties (mechanical and shrinkage) and some localization problems are computed and illustrated.

wood / anatomy / image / X-ray / finite element mesh

Résumé – Utilisation de l'imagerie X pour la prédiction du bois de chêne : **représentation, homogénéisation et localisation. Partie I** : **Imagerie X numérique et représentation par éléments finis.** Cet article est la première partie d'une modélisation complète dans laquelle le bois est considéré comme un matériau composite bidirectionnel. Nous proposons une approche déterministe permettant de prédire les propriétés élastiques et de retrait du chêne dans le plan transverse à partir des propriétés locales des tissus qui le composent et de leur distribution spatiale. Cette première partie (Part I) est dédiée aux processus de description du matériau qui permettront ensuite d'effectuer les calculs de prédiction. Le plan ligneux particulier du chêne a conduit à définir un volume élémentaire d'étude composé d'un accroissement annuel délimité dans la direction tangentielle par les gros rayons ligneux. Un dispositif d'imagerie X numérique de hautes résolutions spatiale et quantitative a été développé afin d'accéder au plan d'organisation des tissus. Un processus de segmentation et de description des contours des différentes plages de tissu (rayons ligneux, gros vaisseaux, etc.) a ensuite été mis au point. Il permet d'utiliser l'image obtenue et de créer un maillage par éléments finis représentatif du matériau composite. La flexibilité de la méthode permet d'optimiser le nombre d'éléments triangulaires tout en conservant une description fidèle de la structure naturelle. La seconde partie (Part II) présentera le principe du calcul d'homogénéisation réalisé à partir des maillages précédemment obtenus (Part I). Les calculs des propriétés macroscopiques (mécanique élastique + retrait) du matériau et du champ de microcontraintes seront illustrés par quelques exemples sur des structures réelles de bois de chêne.

bois / anatomie / image / rayons X / maillage par éléments finis

1. INTRODUCTION

Given the biological activity of a tree, wood is a material with highly variable properties. Its appearance and properties highly depend on the species, but also on biological diversity and on growth conditions. Indeed, wood properties depend on the tree, its age, on the position within the tree, etc. Biometrics is widely used to address this variability.

* Correspondence and reprints
Tel.: 03 83 39 68 86; fax: 03 83 39 68 47; e-mail: badel@engref.fr

Satisfactory results have been obtained that predict wood properties using simple macroscopic values, such as density, ring width and age. Nevertheless, the residual part of these predictions remains large: the scattering of experimental data is such that a factor two can be observed on the parameter measured for a same set of predictive parameters.

In the present work, we propose a deterministic approach based on a mechanical formulation where wood is considered as a natural heterogeneous material (*figure 1*). As a consequence, the individual properties and spatial organisation of its components have to be considered in the understanding of the macroscopic physical and mechanical behaviours. This implies that information has to be collected at the microscopic scale rather than at the macroscopic one to obtain a good prediction of material properties. Several scales of observation are conceivable. For example, at the cell level in the transverse plane, several authors have modelled mechanical properties using the arrangement of the cells [9, 12]. Ando [1] has explained the compression behaviour in the transverse plane by the anatomy at this cell level and Koponen [16] has proposed quite good explanations of shrinkage properties.

At a smaller scale, structural parameters such as microfibrils have long been known [6] to be involved in cell wall properties. Their orientation in the different layers is extensively studied. Recent papers [5, 11, 19] have confirmed that they played a role in the longitudinal and transverse mechanical or shrinkage properties.

In order to understand the relationships between the anatomical structure and the macroscopic properties at the annual ring level many authors have used one kind of cells (for example, tracheids in earlywood in softwood). Gibson and Ashby [10] have studied the influence of the cell geometry. Kifetew [15] or Watanabe [21] have proposed methods to evaluate the effect of their spatial organisation on mechanical and shrinkage properties. Other authors have studied the influence of the cell wall thickness on the tissue behaviour.

This two-part paper deals with a heterogeneous wood. It shows how the spatial distribution of tissues from one annual ring of oak can be collected and how this information can be taken into account to predict shrinkage and mechanical properties in the radial-tangential plane. Homogenisation techniques are appropriate to study heterogeneous materials. This deterministic approach requires two kinds of local information (*figure 2*):

1 – Characterisation of microscopic components: the intrinsic properties of each component of the composite material have to be determined. The difficulties lie in the experimental evaluation of the local mechanical and shrinkage properties [7]. In the case of wood, given its biological origin, these different components never exist alone. In the present work, small samples of ray cells, fibre zones, etc., were isolated. Then specific devices were developed to perform experiments on extremely small samples (a few hundred micrometers). The following experiments were carried out:

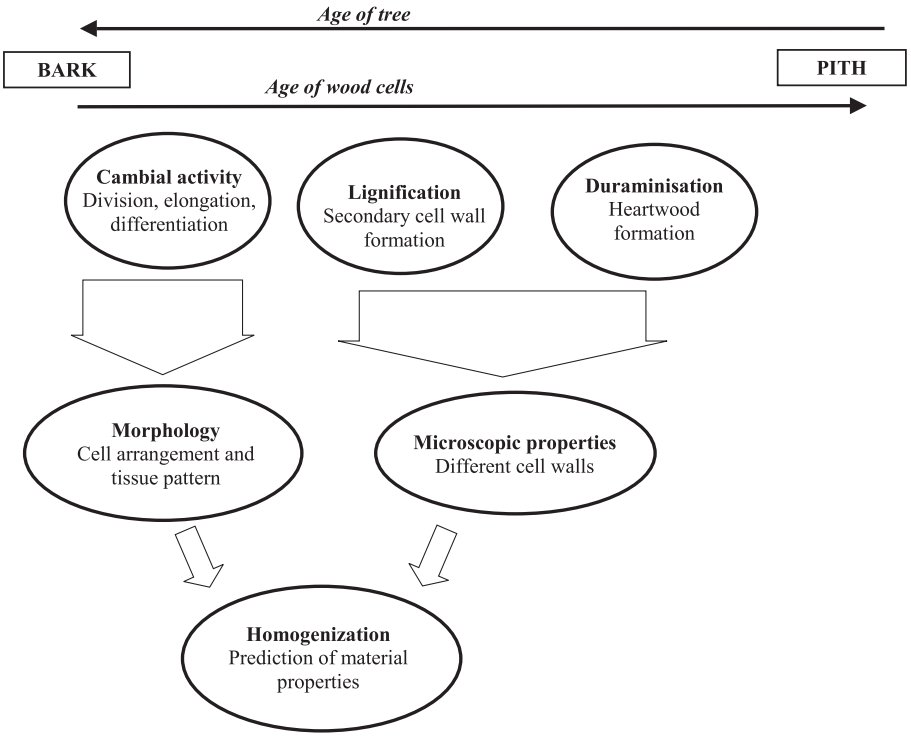

Figure 1. The secondary growth of the tree: from tree biology to wood material.

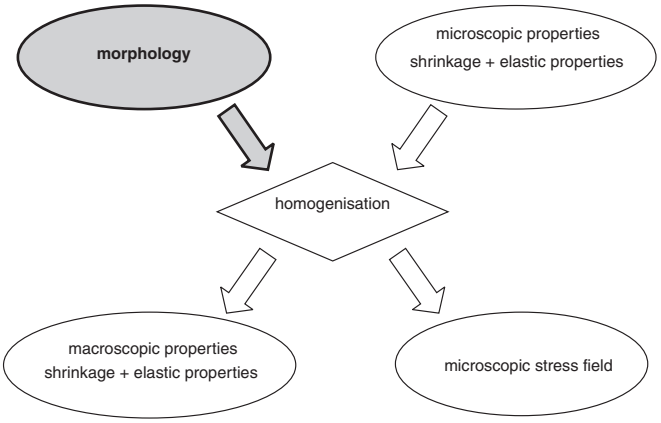

Figure 2. How the knowledge of the intrinsic properties of components and their spatial distribution in the composite material make it possible to compute its behaviour.

– tensile tests under microscope to evaluate the Young modulus and Poisson's ratio values in the transverse plane [3];

– shrinkage tests with X-ray images to obtain shrinkage values in the transverse plane [4].

2 – Geometrical description of the material structure: the spatial organisation of the components of the heterogeneous material have to be observed and qualitatively characterised [7, 8, 15, 17, 21].

In homogenisation problems, the definition and description of the elementary representative volume is a key step. The methodology and the application to an annual ring of oak are the aim of Part I.

The complete study is presented in two papers as follows:

PART I:

– **X-ray imaging**: A new **digital X-ray imaging device** was developed to describe the actual spatial organisation of tissues in one annual ring in the transverse plane.

– **F.E. representation**: A complete mesh process was devised. Image segmentation and partitioned boundaries were performed. Then, controlled equalisation of these boundaries made it possible to build a finite element mesh of the actual structure.

PART II:

Using homogenisation formulation, we used a software, called MophoPore and developed by Perré [18]. It makes it possible to compute the macroscopic properties of the heterogeneous structure from the previous meshes and to visualise the microscopic stress field due to a macroscopic load.

Several examples are presented to illustrate some of the possibilities of scientific applications.

2. X-RAY IMAGING

Keeping in mind the objective of this work, i.e. to better predict the wood properties according to its variable structure, determining and the describing the representative elementary volume (R.E.V.), is a major step. In particular, it is absolutely necessary to deal with the actual anatomy, rather than with averaged or idealised morphology description. According to the observation of oak anatomy, it becomes evident that the most promising change of scale should consider the tissue arrangement (ray cell, fibre zone, etc.) as microscopic scale and the annual growth ring as macroscopic scale. At this scale, the variations in the longitudinal direction are very small. This justifies that, in a first approximation, we consider the usual 2D character of the material in our model. More specifically, the R.E.V. used in this work consists of one annual ring bounded in the tangential direction by large zones of ray cells (*figure 3*).

Remark: for the R.E.V. to be representative of the macroscopic material, the area of interest in the tree must have similar annual rings. The reader has to keep in mind this assumption throughout this work, especially in Part II.

The first tests of image processing proved that anatomical views with an optical microscope are not suitable for easy image segmentation (we tested both transmitted light on microtome cross-sections and reflected light on polished samples). This is one of the main justifications for the development of a specific X-ray imaging device. Because materials absorb X-ray according to their chemical composition and density, X-ray inspection has been commonly used in wood science for several years to gather local information on the structure [20]. The physical principle consists in determining the attenuation properties (attenuated beam intensity over initial beam intensity ratio) of wood samples.

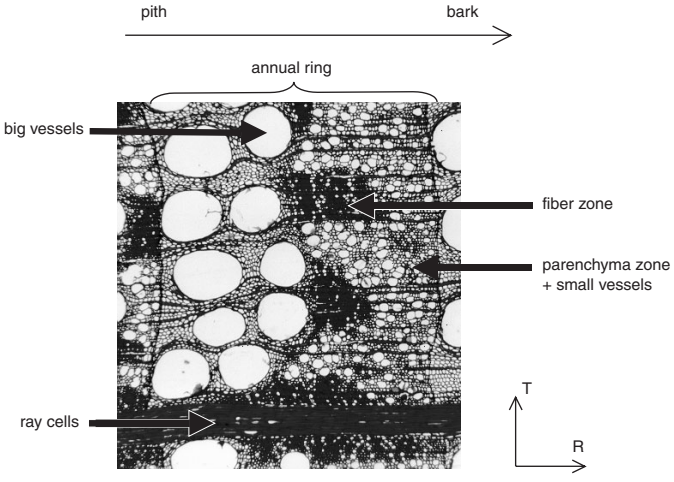

Figure 3. Different tissues of oak shown by optical microscopy in a thin cross-section of wood.

2.1. Design of a digital X-ray imaging device: principle and technical features

X-ray images of wood structure in the transverse plane are performed using thin samples. A cross-section of wood is placed along the X-ray beam. The later goes through the sample in the longitudinal direction and a 2-D detector makes it possible to obtain a cartography of the sample structure in the radial-tangential plane.

The major characteristics of the device are:

– A microfocus X-ray source (Hamamatsu L6731): its specificity is the very small spot size (∅ ~ 8 μm), which makes it possible to place the sample away from the detector system without blurring. Therefore, a magnification can be obtained by simple geometrical projection. The source voltage can vary from 20 to 80 kV and the intensity from 0 to 100 μA.

– A scintillator (Hamamatsu FOP): this element is made of a thin layer (~ 150 μm) of Thallium doped Caesium Iodide (CsI(Tl)). It absorbs the energy of X-ray photons and converts it into visible photons. The layer is set down on a fibre optic plate that guides the light toward the detector.

– A 2-D detector (Princeton Instrument RTEA/CCD-1317K): the detector is a cooled CCD camera. The control of CCD temperature (–35 °C) considerably reduces the noise level. This makes it possible to use acquisition times up to one hour without significant noise. This requirement is due to the low intensity beam of the microfocus X-ray source. The CCD is made of 1317 × 1035 small pixels, $6.8 \times 6.8\ \mu m^2$ each. A computer drives the camera and records the data.

The sample partly absorbs the incident X-ray beam. In order to protect the camera from the residual X-ray beam, the visible light is deviated by a prism (*figure 4*). We devised the device so as to make it very versatile. In particular, the magnification factor (determined by the position of the sample support along the source – detector path) can be easily modified. *Figure 4* depicts the device with × 3 adjustment.

2.2. Image corrections: the advantage of digital images

The relevant information to be measured is the attenuation ratio I/I_0 (I: intensity of the residual beam after going through the sample; I_0: intensity of the incident beam). In the case of polychromatic X-ray beam, this ratio can be calculated as an average value of the attenuation over the energy spectrum:

$$\frac{I}{I_0} = \frac{\int_0^\infty I_0(\lambda) e^{-\mu_m(\lambda)\rho x}\, d\lambda}{\int_0^\infty I_0(\lambda)\, d\lambda} \qquad (1)$$

with λ: wavelength of X-ray; $\mu_m(\lambda)$: absorption coefficient; ρ: density and x: thickness of the sample.

It depends on the chemical composition of the sample, its density, its thickness and the nature of the incident X-ray beam. A raw image (I_R) includes many defaults. A whole image processing protocol is required to approach the theoretical ratio proposed in equation (1). At first, the capture of a complementary image, the "Background" (I_B), without X-ray illumination, allows offset and average noise level be to evaluated and subtracted. A second image is obtained without sample but with X-ray illumination. It corresponds to the

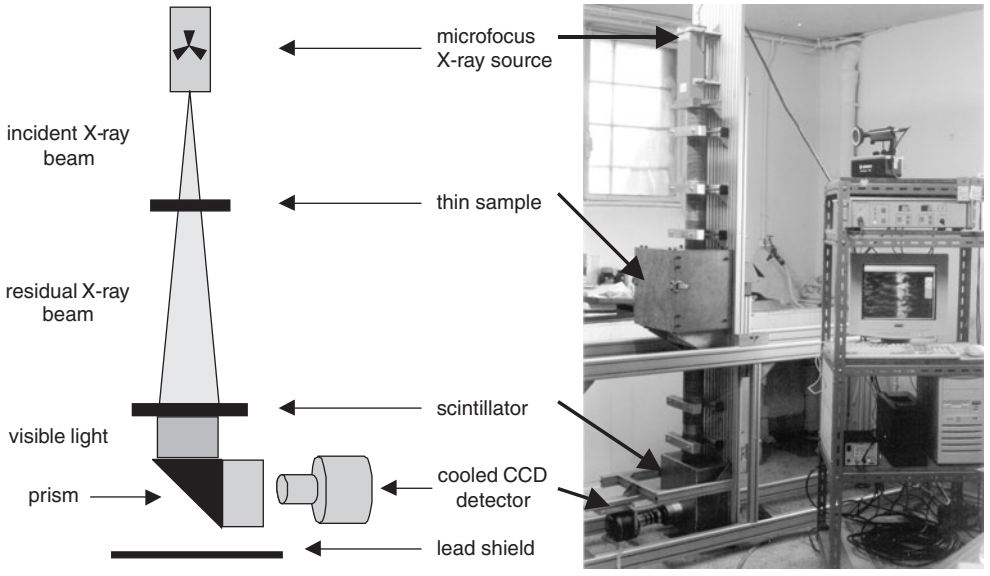

Figure 4. Schematic diagram and overview of an X-ray device for microscopic inspection of wood. The energy of the residual X-ray beam is converted into visible light. The detection is performed by a cooled CCD camera.

intensity of the incident X-ray beam. This image (I_F), called "Flatfield", aims at accounting for the spatial non-uniformity of the X-ray and optical chain. Finally the grey level of each pixel is calculated as follows:

$$G(i, j) = \frac{I_R(i, j) - I_B(i, j)}{I_F(i, j) - I_B(i, j)} \quad (2)$$

where I(i, j) is the intensity of the point with co-ordinates i, j. The "G" value corresponds, for each point, to the I/I_0 ratio (equation (1)). It ranges from 0 (total attenuation of X-ray beam by the sample) to 1 (no attenuation).

The effect of cosmic particles (very high-energy photons coming from space) cannot easily be cancelled and requires several images: a median temporal filter using the same pixel location of successive views of the sample makes it possible to remove the extreme values.

Figure 5 illustrates the "Flatfield" correction step. As the intensity is distinctly higher in the centre of the detector (image A), the "Flatfield" image (image B) makes it possible to take this effect into account. Dark areas correspond to high attenuation values and brightest values (without sample or big vessels) to no attenuation (G = 1).

2.3. Spatial and quantitative resolution

2.3.1. Spatial resolution

Several protocols are available to evaluate the spatial resolution of an imaging system. They are all equivalent [13] and attempt to determine the modulation transfer function (M.T.F.) that characterises the response of the device to a Dirac stimulation. In the present work, we used the bar/space method [14]. It consists in imaging a lead-bar chart of known spatial frequencies (*figure 6*) and to measure a contrast between strong and low absorption lines. *Figure 6* shows an X-ray image of the pattern and represents the evolution of M.T.F. according to spatial frequency (given in line pairs mm^{-1}). The spatial resolution is given by the value where M.T.F. reaches the 10% limit. Below this value, it is admitted that the eye cannot distinguish a detail anymore.

Assuming that spatial resolution varies according to the magnification rate, two cases are plotted. For example, for a × 3 magnification, the accuracy is 18 line-pairs mm^{-1}, which corresponds to 27 µm. For the operator, choosing the magnification rate results from a compromise between the spatial accuracy and the field of the image. For a × 1 magnification, the field is about 3 cm.

2.3.2. Quantitative resolution

The quantitative resolution characterises the accuracy of the device for the I/I_0 ratio determination. A comprehensive study has been carried out to define the best operating conditions [2]. Noise has been experimentally evaluated. Measurements show that it varies essentially as the square root of counted photons, regardless of parameters such as intensity,

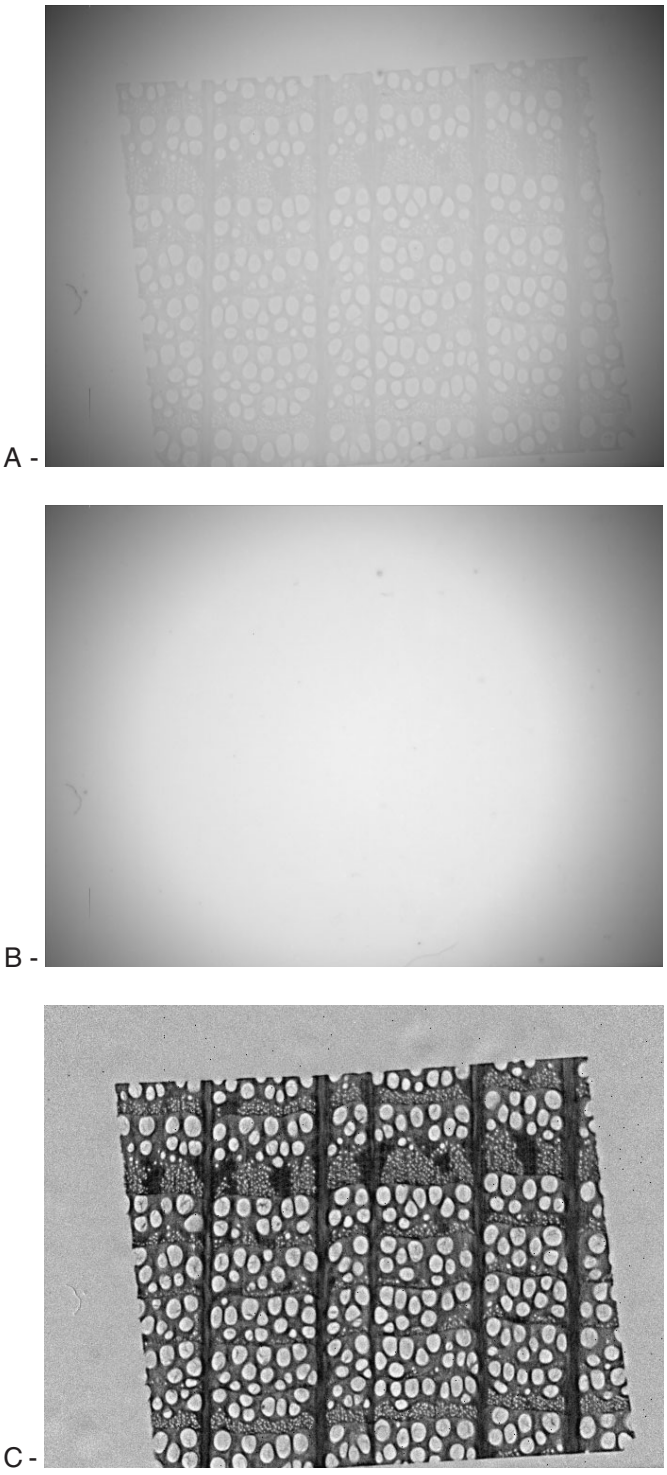

Figure 5. Flatfield correction. Image (C) results from the division of raw image (A) by Flatfield (B). Flatfield represents the incident beam intensity and image (C) corresponds to the I/I_0 ratio. Values range between 0 (total attenuation) and 1 (no attenuation in vessels). Magnification × 2.

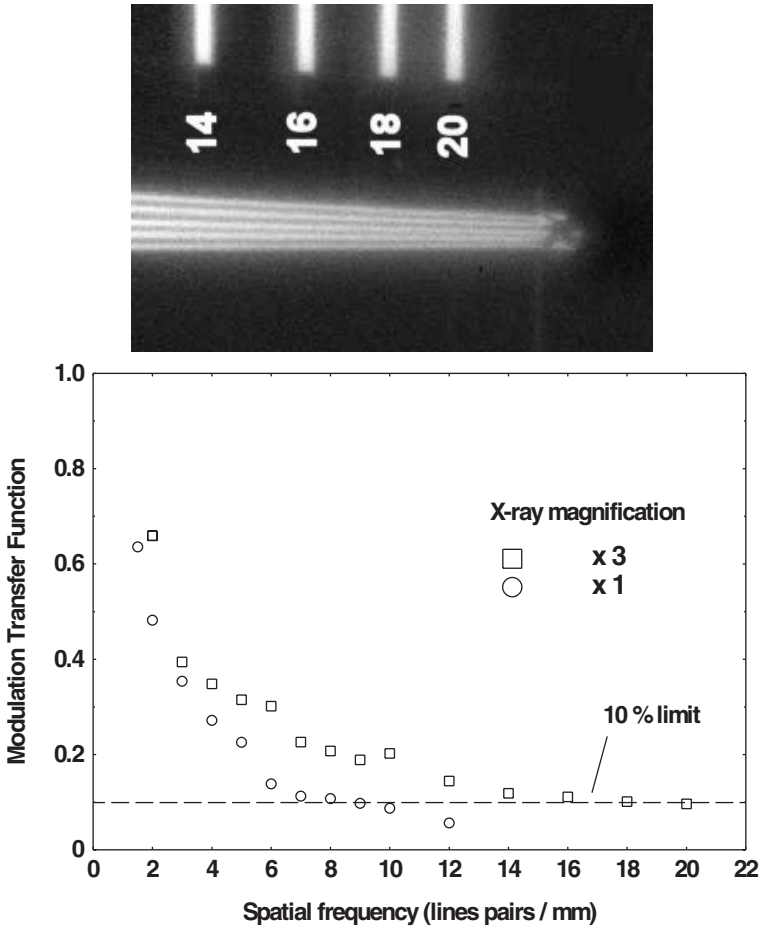

Figure 6. Evaluation of the modulation transfert function using an X-ray image of the bar/space pattern of known spatial frequencies (left). The spatial resolution of the device is given by the 10% limit. Results are presented for two different X-ray magnifications.

voltage or exposure time (*figure 7*). It mainly results from the principle of X-photon production that is a statistic phenomenon and follows a Poison's law. Finally, although high energy X-particles are less attenuated by wood, it is always recommended to use a high voltage because of the higher incident flux. This is one fundamental difference with classic radiographic films that would reach saturation. Typical operating conditions make it possible to obtain a high accuracy image with only a few percents of attenuation at 70 kV.

Figure 5 shows an example with a × 2 magnification for a field of vision at the annual ring level. In order to illustrate the performance of the device in terms of quantitative resolution, we conducted a specific test at the cellular level. In that case, we chose a simple cellular organisation with only one kind of tissue (spruce). The sample was a thin slice (around 50 µm thick) prepared with a sledge microtome. Cell walls absorbed less than 1% of the X-ray beam. The perfect linearity of the detector, together with the spatial corrections, made it possible to obtain a very good Signal-Noise ratio using a long exposure time (12 hours in this case). Thanks to a great

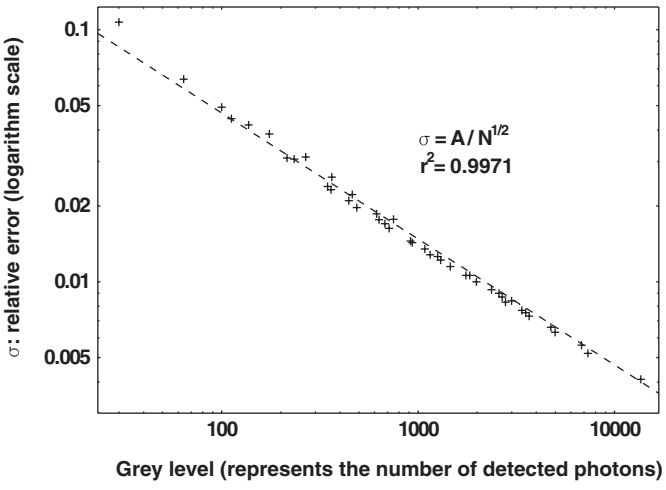

Figure 7. Variation of the experimental noise according to the number of photons. The relative noise (σ) represents the percentage of noise compared with the recorded signal.

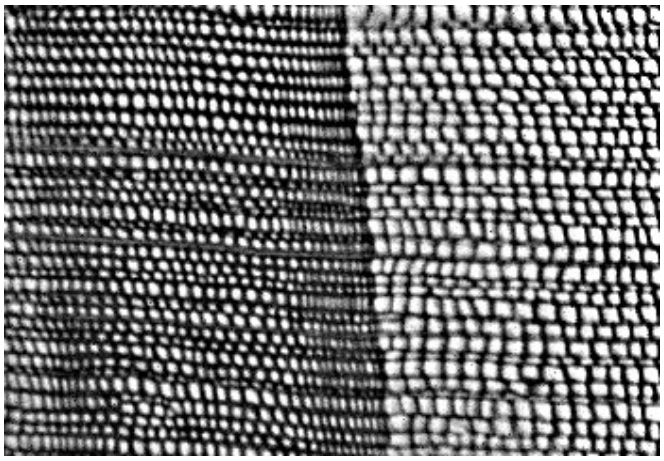

Figure 8. Accuracy of I/I_0 measurement. This X-ray image is an example of detection performance. The sample is a very thin slice of wood (≈ 50 µm). The cell walls absorb less than 1% of the incident X-ray beam intensity. The quality of the image (contrast between lumen and cell wall) involves a great number of X-photons to be detected. The experimental X-ray conditions are: ΔV = 70 kV, I = 95 µA, exposure time: 12 h.

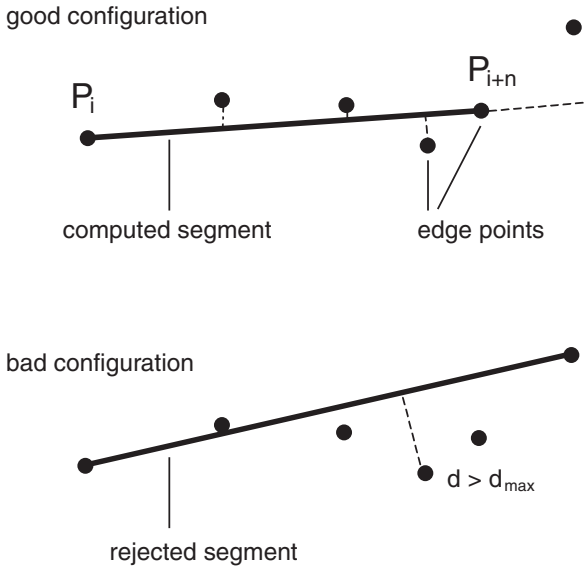

Figure. 9. Edge approximation. The segment replaces the edge points if the distance of each removed point to this computed segment is smaller than d_{max}.

magnification (× 18), the cellular structure of wood is easily detected in this image (*figure 8*).

3. REPRESENTATION BY FINITE ELEMENTS

The theoretical formulation of homogenisation techniques will be presented in detail in Part II. In this "representation" part, we need to keep in mind that computations are performed for a representative elementary volume (R.E.V.). In the case of oak wood in the transverse plane, we define this volume as an annual ring limited in the tangential direction by large ray cells. This heterogeneous volume is composed of four main components: big vessels, fibre zone, ray cells and parenchyma zone.

The following procedure is used to build suitable F.E. meshes from the X-ray images:

3.1. From X-ray image to vector-valued information

The complete procedure is divided into five steps:

(a) image segmentation: using image analysis tools (threshold, erosion, reconstruction, hole fill, etc.) the areas of the four main components of annual ring are separated;

(b) vectorisation: the contour of each zone is then defined as a list of consecutive pixels;

(c) segment chaining: the previous contours are partitioned and approximated by chains of segments. The procedure starts at one point, let say P_i, of the contour and consists in removing as much pixels as possible. This is a dichotomy process: points P_{i+1} to P_{i+n-1} are cancelled if all of them are close enough from segment $[P_i, P_{i+n}]$ (*figure 9*). The operator defines this maximal authorized distance, or "error", that is the same along the contour. This method makes it possible to control the difference of shape between description by points and description by segments. This process minimises the segment number but produces segments of variable lengths;

(d) equalisation of contours: for each area, the length of the segments is controlled. A specific process computes a new contour in order to obtain regular partition. This procedure allows the F.E. refinement to be controlled for each tissue area. The principle consists in following the irregular segments with a circle to define the position of the next point on the contour. *Figure 10*, (A) represents the irregular boundary (initially 4 segments). Case (B) illustrates a refined partition (16 segments are computed) and case (C) represents an unrefined partition (only 4 segments are computed);

(e) mesh generation: a free software (Easymesh©) uses the previous data to build the final triangular F.E. mesh.

Remark: the homogenisation formulation used in Part II assumes that the macroscopic material is periodic (see previous remark and Part II). The consequence is that the displacements of nodes on two opposite sides of the mesh have to be identical. This leads to force the position of each node on the 4 sides of the mesh to ensure this correspondence.

3.2. Examples of mesh refinement facilities

The equalisation step makes it possible to control for each area the refinements of contours, and therefore the number of triangular elements in the 2D-mesh. The satisfactory

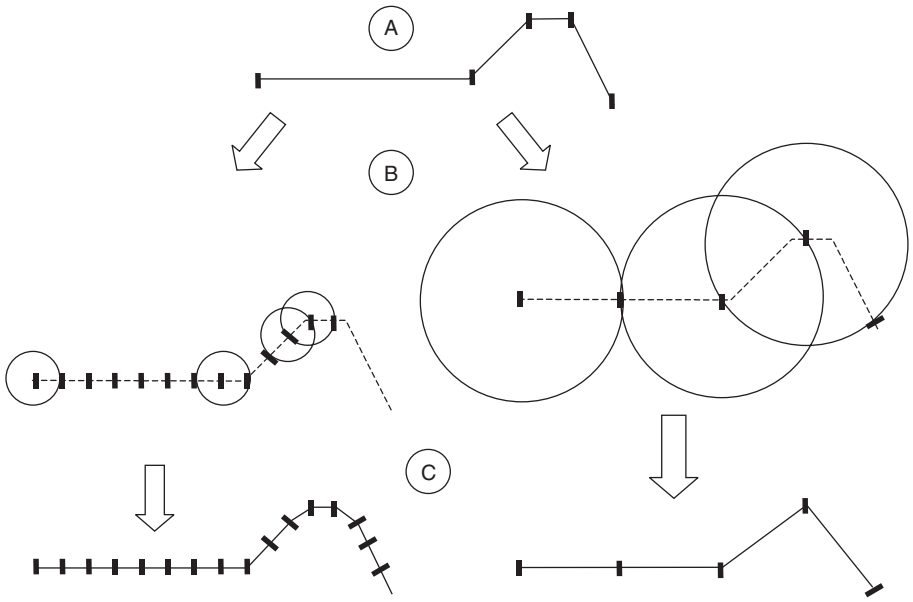

Figure 10. Contour equalisation. (A) is the initial irregular boundary (4 segments). The advance of the circle on the initial segments (B) defines a new regular partition (C). Left part illustrates a refined case and right part shows an unrefined process.

optimisation consists in searching a compromise between good material description and computing time. *Figure 11* depicts the full representation process; from X-ray image to the F.E. mesh. Three cases illustrate the mesh refinement facilities:

– Unrefined description involves only 336 degrees of freedom and all the areas are badly represented. Especially, the smallest vessels are removed and the shape of the biggest is limited to a triangle. Even if homogenisation computations are very fast the result cannot be representative of the original wood structure.

– The second case shows a better representation of morphology. The sides of triangles are three times smaller than previously. Several vessels appear and contours of the fibre zones are already well described. A total of 2786 degrees of freedom are necessary.

– The last example illustrates a highly refined case. Even the smallest vessels are represented and round shapes are well fitted. The sides of the triangles are twice as small as in the previous case and 9848 degrees of freedom are used.

These examples lead to assume that optimising the size elements can be obtained for each kind of tissue. Vessels require high refinement in order to fit with their small and round shape. Such a fine description is not useful for bigger tissues like fibre zones. Using an appropriate size for triangular elements makes it possible to reduce the total number of degrees of freedom while preserving the quality of wood description. In practice, this possibility will be used during the building of mesh in order to optimise the size of elements according to the size of the tissue zone.

4. CONCLUSIONS AND PROSPECTS

This first part deals with the observation and representation of the anatomical morphology of wood. Assuming that oak wood is a very heterogeneous material made of different components, their spatial organisation has to be taken into account for a better understanding of its shrinkage and mechanical properties. Accordingly, several experimental and computer tools were developed to observe the anatomical structure of oak wood and to translate this information into computing data suitable for further computations.

First, a new X-ray imaging device was developed. It is based on microfocus X-ray source and CCD camera. The small size of the spot allowed great magnifications. It compensates for the spatial resolution of digital detectors that is not sufficient actually for wood anatomy imaging. Digital detection makes it possible to obtain a very high accuracy, even with very thin wood slices. This device was conceived to be very adjustable in order to fit different scales of observation. In the present study, it provided images of wood cross-sections at the annual ring level. X-ray images of oak structure in the transverse plane were obtained with 27 µm resolution. Besides the apparatus was designed to follow the quick technical progress. Higher resolutions are already available.

The second step is devoted to the generation of finite element mesh from the previous X-ray image. A computing process, including image analysis, was devised. The good Signal-Noise ratio of the X-ray image makes it possible to separate four different anatomical areas (big vessels, ray cells, fibre zones and parenchyma zones). At this step, the heterogeneous material is defined and a complete procedure

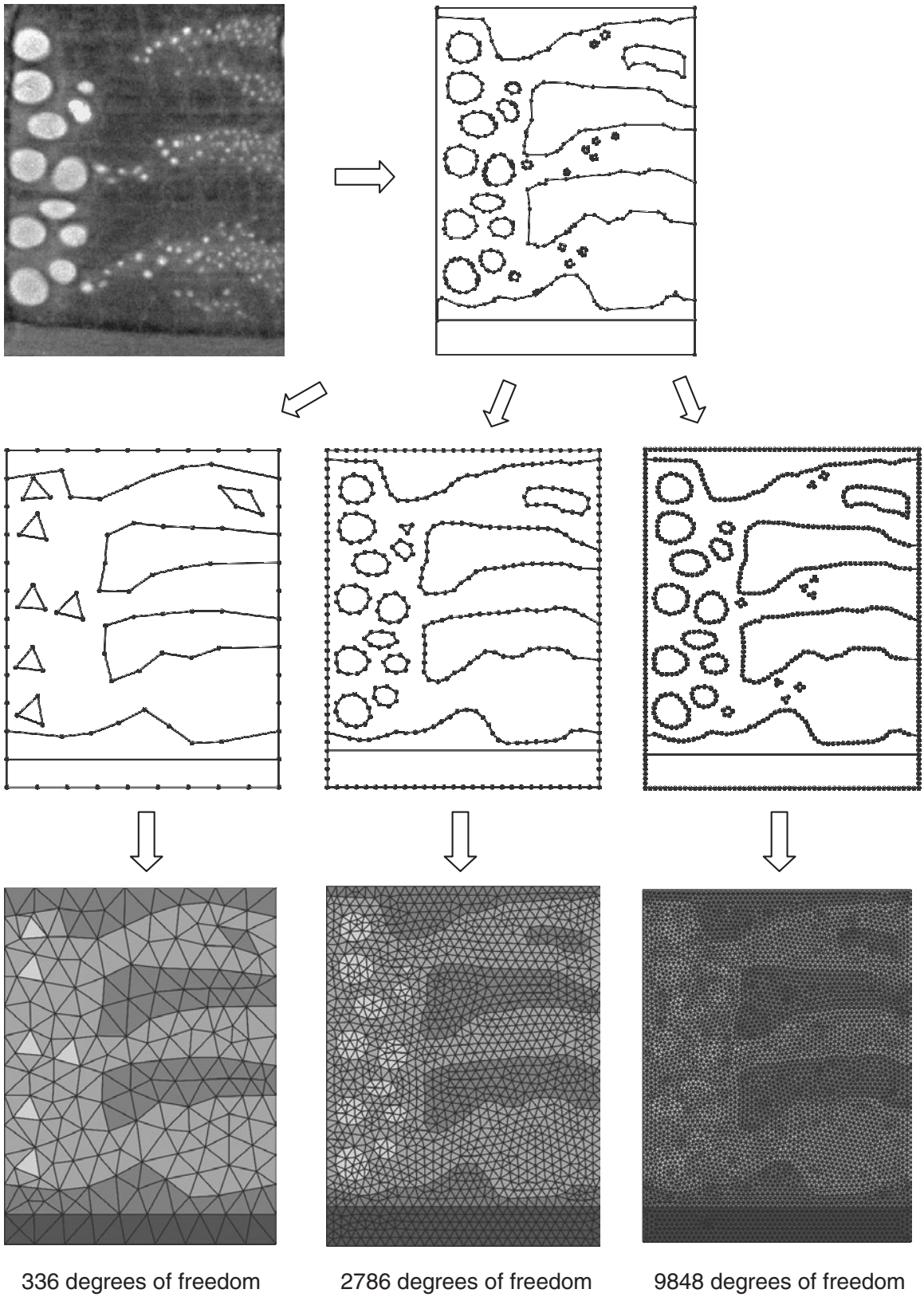

Figure 11. The main step of finite element representation. The tissue areas are isolated from X-ray image and boundaries are detected. The equalisation step allows the refinement to be controlled before the building of finite element mesh.

makes it possible to build a triangular F.E. mesh while controlling the description accuracy. This new structure becomes the input data for next shrinkage and mechanical modelling.

Assuming that local properties of each tissue have been evaluated previously, Part II will present homogenisation techniques. Macroscopic properties of this heterogeneous structure will be computed and local cartography of local stress due to shrinkage will be proposed.

Acknowledgement: The authors thank Mrs Huber for providing the microtome slice used to illustrate the performance of the digital X-ray device.

REFERENCES

[1] Ando K., Onda H., Mechanism for deformation of wood as a honeycomb structure. I: Effect of anatomy on the initial deformation process during radial compression, J. Wood Sci. 45 (1999) 120–126.

[2] Badel É., Détermination des propriétés élastiques et du retrait d'un cerne annuel de chêne dans le plan transverse : description de la morphologie, mesures des propriétés microscopiques et calculs d'homogénéisation, Doctoral thesis, ENGREF, Nancy, 1999.

[3] Badel É., Perré P., Détermination des propriétés élastiques d'éléments individuels du plan ligneux du chêne par des essais de traction sur microéprouvettes, Ann. For. Sci. 56 (1999) 467–478.

[4] Badel É., Perré P., Using an X-ray imaging device to measure the swelling coefficients of a group of wood cells, NDT&E International 34 (2001) 345–353.

[5] Bergander A., Salmen L., Variations in transverse fibre wall properties: relations between elastic properties and structure, Holzforschung 54 (2000) 654–660.

[6] Boutelje J.B., The relationship of structure to transverse anisotropy in wood with reference to shrinkage and elasticity, Holzforschung 16 (1962) 33–46.

[7] Clair B., Despaux G., Chanson B., Thibaut B., Utilisation de la microscopie acoustique pour l'étude des propriétés locales du bois : étude préliminaire de paramètres expérimentaux, Ann. For. Sci. 87 (2000) 335–343.

[8] Diao X., Furuno T., Uehara T., Analysis of cell arrangements in softwoods using two-dimensional fast Fourier transform, Mokusai Gakkaishi 42 (1996) 634–641.

[9] Farruggia F., Perré P., An explanation of mechanical behaviour of early wood (*Picea abies*) in the transverse plane based only on the arrangement of the cells, Plant biomechanics, Conference Proceedings (1997) 215–221.

[10] Gibson L.J., Ashby M.F., Cellular solids, structure and properties, Pergamon Press, 1988.

[11] Harrington J.J., Astley R.J., Brocker R.E., Modelling the elastic properties of softwood. Part I, the cell wall lamellae, Holz Roh- Werkst. 56 (1998) 43–50.

[12] Harrington J.J., Brocker R., Astley R.J., Modelling the elastic properties of softwood. Part II: the cellular microstructure, Holz Roh- Werkst. 56 (1998) 37–41.

[13] Kaftandjian V., Zhu Y.M., Roziere G., Peix G., Babot D., A comparison of the ball, wire, edge and bar/space pattern techniques for modulation transfer function measurements of linear X-ray detectors, J. X-ray Sci. Technol. 6 (1996) 205–221.

[14] Kaftandjian V., Zhu Y.M., Peix G., Babot D., Contrast transfer function measurement of X-ray solid state linear detectors using bar/space pattern methods, NDT&E International 29 (1996) 3–11.

[15] Kifetew G., The influence of the geometrical distribution of cell wall tissues on the transverse anisotropic dimensional changes of softwood, Holzforschung 53 (1999) 347–349.

[16] Koponen S., Toratti T., Kanerva P., Modelling elastic and shrinkage properties of wood based on cell structure, Wood Sci. Technol. 25 (1991) 25–32.

[17] Lichtenegger H., Reiterer A., Tschegg S., Fratzl P., Imaging of the helical arrangement of cellulose fibrils in wood by synchrotron X-ray microdiffraction, J. Appl. Crystalogr. 32 (1999) 1127–1133.

[18] Perré P., The use of homogeneisation to simulate heat and mass transfer in wood: towards a double porosity approach plenary lecture, International Drying Symposium, published in Drying'98, 1998, 57–72.

[19] Person K., Micromechanical modelling of wood and fibre properties, Report TVSM–1013, Doctoral thesis, Lund Univesity, 2000.

[20] Polge H., Établissement des courbes de variation de la densité du bois par exploration densitométrique de radiographies d'échantillons prélevés à la tarière sur des arbres vivants, Ann. Sci. For. 23 (1966).

[21] Watanabee U., Shrinking and elastic properties of coniferous wood in relation to cellular structure, Doctoral thesis, Kyoto University, 1998.